Transcriptomics and metabolomics study in mouse kidney of the molecular mechanism underlying energy metabolism response to hypoxic stress in highland areas

YUJIE GAO, QIFU LONG, HUI YANG, YING HU, YUZHEN XU, CHAOQUN TANG, CUNLIN GU and SHENG YONG

Department of Basic Medicine, School of Medicine, Qinghai University, Xining, Qinghai 810016, P.R. China

Received May 15, 2023; Accepted August 25, 2023

DOI: 10.3892/etm.2023.12232

Abstract. Exposure to hypoxia disrupts energy metabolism and induces inflammation. However, the pathways and mechanisms underlying energy metabolism disorders caused by hypoxic conditions remain unclear. In the present study, a hypoxic animal model was created and transcriptomic and non-targeted metabolomics techniques were applied to further investigate the pathways and mechanisms of hypoxia exposure that disrupt energy metabolism. Transcriptome results showed that 3,007 genes were significantly differentially expressed under hypoxic exposure, and Gene Ontology annotation analysis and Kyoto Encyclopaedia of Genes and Genomes (KEGG) enrichment analysis showed that the differentially expressed genes (DEGs) were mainly involved in energy metabolism and were significantly enriched in the tricarboxylic acid (TCA) cycle and oxidative phosphorylation (OXPHOS) pathway. The DEGs *IDH3A*, *SUCLA2*, and *MDH2* in the TCA cycle and the DEGs *NDUFA3*, *NDUFS7*, *UQCRC1*, *CYC1* and *UQCRFS1* in the OXPHOS pathway were validated using mRNA and protein expression, and the results showed downregulation. The results of non-targeted metabolomics showed that 365 significant differential metabolites were identified under plateau hypoxia stress. KEGG enrichment analysis showed that the differential metabolites were mainly enriched in metabolic processes, such as energy, nucleotide and amino acid metabolism. Hypoxia exposure disrupted the TCA cycle and reduced the synthesis of amino acids and nucleotides by decreasing the concentration of cis-aconitate, α-ketoglutarate, NADH, NADPH and that of most amino acids, purines, and pyrimidines. Bioinformatics analysis was used to identify inflammatory genes related to hypoxia exposure and some of them were selected for verification. It was shown that the mRNA and protein expression levels of *IL1B*, *IL12B*, *S100A8* and *S100A9* in kidney tissues were upregulated under hypoxic exposure. The results suggest that hypoxia exposure inhibits the TCA cycle and the OXPHOS signalling pathway by inhibiting *IDH3A*, *SUCLA2*, *MDH2*, *NDUFFA3*, *NDUFS7*, *UQCRC1*, *CYC1* and *UQCRFS1*, thereby suppressing energy metabolism, inducing amino acid and nucleotide deficiency and promoting inflammation, ultimately leading to kidney damage.

Correspondence to: Professor Sheng Yong, Department of Basic Medicine, School of Medicine, Qinghai University, 251 Ningda Road, Xining, Qinghai 810016, P.R. China
E-mail: yongsheng@qhu.edu.cn

Key words: kidney, hypoxia, tricarboxylic acid cycle, oxidative phosphorylation, transcriptomics, metabolomics, mitochondrial dysfunction, inflammation

Introduction

After the human body rises to the plateau area at an altitude of 2,500 m, the partial pressure of oxygen (PaO_2) decreases with increasing altitude, producing a low-pressure hypoxic situation. The inability of the human body to adapt to low-pressure and hypoxic environments can lead to tissue hypoxia, followed by acute plateau reactions, such as plateau pulmonary or cerebral oedema, and acute altitude sickness (1). Acute and prolonged exposure to low-pressure and hypoxic environments can lead to the generation of reactive oxygen species (ROS), which accelerates with increasing altitude (2). Relatively high levels of ROS may cause oxidative damage to tissues or induce apoptosis under immune defence or pathological conditions (3). It is estimated that >140 million individuals worldwide live at altitudes >2,500 m (4). Therefore, it is important to study the molecular mechanisms of tissue systems in response to hypoxic stress at high altitudes in workers and sojourners in high-altitude areas.

The kidney is a highly metabolic organ that requires a large amount of adenosine triphosphate (ATP) to maintain the energy needed for water and solute reabsorption. Abnormal energy production or utilisation can lead to cell dysfunction and death (5). At the centre of cellular bioenergetics, mitochondria serve a key role in the regulation of cellular metabolism (6). In response to hypoxic environments, mitochondria were reported to adjust their metabolism in different ways, including exchanging or modifying subunits of the respiratory chain, reducing oxidative phosphorylation (OXPHOS), tricarboxylic acid (TCA) cycle intermediates, adapting to

ROS production and reducing β-oxidation (7). A recent study showed that impaired energy metabolism is characterised by ATP deficiency and increased ROS (8), while a previous study showed that increased ROS ultimately leads to mitochondrial dysfunction by inducing mitochondrial oxidative damage (9). In addition, mitochondrial ROS production plays a key role in the development of diabetic nephropathy and inhibiting excessive mitochondrial ROS production can improve tubular oxidative damage (10). It was previously reported that energy metabolism dysfunction is a key factor in the pathogenesis of acute kidney injury (AKI) (5). AKI is widely recognised as an important risk factor for the development and progression of chronic kidney disease (CKD) (11-13). Dysregulation of mitochondrial homeostasis, changes in bioenergetics, and organelle stress crosstalk can lead to the transformation of AKI into CKD (14). Taken together, dysfunction of energy metabolism can induce kidney tissue damage.

The TCA cycle and OXPHOS are important sources of cellular energy and are involved in numerous cellular metabolic pathways (15,16). Exposure to hypoxia inhibits the TCA cycle pathway and converts the glycolytic pathway into the primary metabolic pathway that generates available energy (17). Therefore, further investigation is required regarding changes to energy metabolism mechanisms induced by hypoxia through the TCA cycle with the OXPHOS pathway.

To improve the comprehension of the effect of hypoxic exposure on mouse kidney tissue, a plateau hypoxia animal model was constructed in the present study. Kidney tissue morphology was observed using haematoxylin and eosin (H&E) staining. Illumina transcriptome sequencing and liquid chromatography-tandem mass spectrometry (LC-MS/MS) non-targeted metabolomics techniques were used to identify differentially expressed genes (DEGs) and significantly different metabolites (SDMs) between experimental and control groups ($P<0.05$). The mechanism by which hypoxia inhibits energy metabolism in kidney tissues was explored using the TCA cycle and OXPHOS. Furthermore, inflammation-related genes (IRGs) were screened using the Ensembl database and combined with DEGs to analyse the possible effects of hypoxia on inflammation. The present study clarified that hypoxia-induced alterations in renal energy metabolism and that changes in energy metabolism induced inflammation.

Materials and methods

Experimental animals. Six- to eight-week-old specific pathogen-free (SPF) male C57BL/6 mice with a body mass of 18±2 g were purchased from the Experimental Animal Centre of the Department of Medicine, Xi'an Jiaotong University [animal production license no. SYXK (Shaanxi) 2020-005]. The research institute is located in Xining, China at an altitude of 2,200 m; in order to provide a natural normoxic and hypoxic condition, mice were randomly divided into two groups (five mice per group). The control group raised at the Experimental Animal Centre of the Department of Medicine, Xi'an Jiaotong University (Xi'an, China) at an altitude of 400 m, was named the plain normoxia (PKC) group. The plateau hypoxia (HKT) group was raised in the Experimental Animal Room of the People's Hospital of Maduo County, Guoluo Tibetan Autonomous Prefecture (Xining, China), at an altitude of 4,200 m. All animals were provided with free access to food and water. The ambient temperature was 18-25˚C, and the relative humidity was 40-50%. In the process of animal feeding and experimental operation, if mice developed either spontaneous tumors the size of which was >10% of the body weight of mice, incurable skin ulcers, severe shivering, spasm, dyspnea or cyanosis, they were to be euthanized immediately. No mice were euthanized for these reasons in the present study. After 30 days, kidney tissues were aseptically collected from mice; one part was stored in liquid nitrogen, and the other part was fixed with 4% paraformaldehyde at 4˚C for 48 h.

Reagents and instruments. Primers were purchased from Shanghai Sangong Pharmaceutical Co., Ltd. and the TRIzol® RNA extraction buffer was purchased from Invitrogen (Thermo Fisher Scientific, Inc.). The reverse transcription kit PrimeScript™ RT reagent Kit with gDNA Eraser (cat. no. RR047A) and quantitative polymerase chain reaction (qPCR) kit TB Green® Premix Ex Taq™ II (Tli RNaseH Plus; cat. no. RR820A) were purchased from Takara Bio, Inc. The fluorescent qPCR instrument was purchased from Roche Diagnostics GmbH. Antibodies, the ECL chemiluminescent solution and the western blot imaging system were purchased from Proteintech Group, Inc., Thermo Fisher Scientific, Inc. and Vilber Lourmat, respectively.

Measurement of blood gas analysis index and kidney index in mice. After 30 days of modelling, the two groups of mice remained on an empty stomach for 12 h, their fasting weights were measured, and they were anesthetized using 400 mg/kg 10% chloral hydrate. The mice were then fixed on a foam plate to take blood and kidney tissues by laparotomy. After taking 10% chloral hydrate, there was no sign of peritonitis in animals. After laparotomy, 0.2 ml of blood was taken through the abdominal aorta using a heparin anticoagulant needle, and attention was paid to avoid discharging air bubbles in the needle tube and isolating air. Using a PT1000 blood gas analyzer (Wuhan Easy Diagnosis Biomedicine Co., Ltd.), arterial oxygen PaO_2 and blood oxygen saturation (SaO_2) were measured within 15 min. Subsequently, mouse bilateral kidney tissues were removed aseptically, rinsed with pre-cooled saline, and filter paper was used to absorb the water on the kidney surface. Both kidneys were then weighed. The kidney index of the mice was calculated using the following formula: Kidney index=bilateral kidney mass (g)/body mass (g) x100%.

H&E staining of mouse kidney. Mouse kidney tissues were fixed in 4% paraformaldehyde at 4˚C for 48 h, dehydrated in an ethanol gradient, embedded in paraffin and sliced into 5- to 6-μm thick sections. After xylene dewaxing, the slices were stained with hematoxylin for 5 min at room temperature, and after washing, the slices were incubated with eosin for 2 min. Tissue sections were observed by Nikon microscope (Nikon Corporation) and the images were analyzed by Zeiss software (version 2.3; Zeiss AG).

RNA extraction and reverse transcription-qPCR (RT-qPCR). Total RNA in the mouse kidneys was isolated with TRIzol® reagent (Thermo Fisher Scientific, Inc.), and the concentration of RNA was measured with a Nanodrop 2000

Table I. Primers used in the present study.

Gene	Primer sequences (5'-3')	
	Forward	Reverse
β-actin	CATCCGTAAAGACCTCTATGCCAAC	ATGGAGCCACCGATCCACA
IDH3A	AGTTTGATGTTCTTGTCATGCC	GAAGCATCATCACAGCACTAAG
SUCLA2	AAAGGAACATTTACAAGTGGCC	GCTCACAGACCAAAACTTGATT
MDH2	CAAAGAGACGGAATGCACTTAC	CTTTCTTGATGGAGGCTTTCAG
UQCRFS1	AGGTGCCCGACTTCTCTGACTATC	CCGCATAAGCAACACCCACAGTAG
UQCRC1	GGACCTTGCCCAGAAACACTTGAG	CAGTAGAGCGACATGGAGTGAGAC
CYC1	GCCCTTCATTCTGCCGTGAGTG	GGTGTGGTCCAAGGAGGAGAGG
IL12B	ATGTGGAATGGCGTCTCTGTCTG	CAGTTCAATGGGCAGGGTCTCC
IL1B	TCCAGGATGAGGACATGAGCAC	GAACGTCACACACCAGCAGGTTA
S100A8	CTTGAGCAACCTCATTGATGTC	GGAACTCCTCGAAGTTAATTGC
S100A9	GGAAGCACAGTTGGCAACCTTTA	GATCAACTTTGCCATCAGCATCA

spectrophotometer (Thermo Fisher Scientific, Inc.). The RNA was reversed into cDNA using SYBR Green (Takara Bio, Inc.) with Prime Script RT Regent Kit with GDNA Eraser (Takara Bio, Inc.), with the following reaction conditions: 37˚C for 15 min and 87˚C for 5 sec. PCR amplification was performed using cDNA as a template and β-actin as an internal reference. Primer sequences are listed in Table I. All primers used were designed by Shanghai Shenggong Biology Engineering Technology Service, Ltd. The total PCR measured 20 μl, and included 10 μl TB Green® Premix Ex Taq™ II, 6.4 μl ddH_2O, 2 μl template and 0.8 μl of upstream and downstream primers. The thermocycling conditions included pre-denaturation at 95˚C for 30 sec, amplification at 95˚C for 5 sec, 63˚C for 60 sec, and 60 cycles of lysis at 95˚C for 10 sec, 65˚C for 60 sec, 97˚C for 1 sec and finally cooling at 37˚C for 30 sec. The relative expression levels of selected genes in the HKT and PKC groups were quantified using the $2^{-\Delta\Delta Cq}$ method (18).

Western blotting. To extract the total protein of mouse kidney tissues, samples were taken out of the refrigerator at -80˚C and put into a centrifuge tube equipped with protein extraction Lysis Buffer (Beijing Solarbio Science & Technology Co., Ltd.). Kidneys were cut into pieces using sterile surgical scissors and then centrifuged (Beyotime Institute of Biotechnology) at 13,400 x g for 10 min at 4˚C. The supernatant was added to a new aseptic enzyme-free centrifuge tube and the total protein concentration was measured using a BCA kit (Beyotime Institute of Biotechnology). Total protein (30 μg protein/lane) was separated by SDS-PAGE on a 12% gel and transferred onto a nitrocellulose membrane. The membrane was blocked with 5% skimmed milk for 2 h at room temperature and then incubated with primary antibody at 4˚C for 15 h. IDH3A polyclonal antibody (1:500; cat. no. 15909-1-AP; Proteintech Group, Inc.), SUCLA2 polyclonal antibody (1:1,000; cat. no. 12627-1-AP; Proteintech Group, Inc.), MDH2 polyclonal antibody (1:500; cat. no. 15462-1-AP; Proteintech Group, Inc.), UQCRFS1 polyclonal antibody (1:1,000; cat. no. 18443-1-AP; Proteintech Group, Inc.), UQCRC1 polyclonal antibody (1:1,000; cat. no. 21705-1-AP; Proteintech Group, Inc.), CYC1 polyclonal antibody (1:500; cat. no. 10242-1-AP; Proteintech Group, Inc.), NDUFA3 polyclonal antibody (1:200; cat. no. K008505P; Beijing Solarbio Science & Technology Co., Ltd.), NDUFS7 polyclonal antibody (1:1,000; cat. no. 15728-1-AP; Proteintech Group, Inc.), IL12B polyclonal antibody (1:300; cat. no. DF5111; Affinity Biosciences), IL1B monoclonal antibody (1:300; cat. no. BF8021; Affinity Biosciences), S100A8 polyclonal antibody (1:300; cat. no. 15792-1-AP; Proteintech Group, Inc.), S100A9 polyclonal antibody (1:300; cat. no. 26992-1-AP; Proteintech Group, Inc.) and β-actin monoclonal antibody (1:10,000; cat. no. 66009-1-Ig; Proteintech Group, Inc.). The relative expression levels of the target proteins were normalized to those of β-actin. The membranes were washed with TBS containing 0.05% Tween-20 (Beijing Solarbio Science & Technology Co., Ltd.) and then incubated with goat anti-rabbit (1:5,000; cat. no. SA100001-2; Proteintech Group, Inc.) or goat anti-mouse (1:2,000; cat. no. SA100001-1; Proteintech Group, Inc.) secondary antibodies for 1 h at room temperature. The membrane was washed with TBS containing 0.05% Tween-20 five times, each time for 6 min, and the protein bands were visualized using an enhanced chemiluminescence reagent (Thermo Fisher Scientific, Inc.). Protein bands were imaged using a gel imaging analysis system (Vilber Lourmat) and Image J (version 1.80; National Institutes of Health) was used to quantify the protein expression.

Transcriptome sequencing [RNA-sequencing (RNA-seq)] and data processing. Changes in total RNA after high-altitude hypoxia treatment were analysed using transcriptome analysis. The total RNA of mouse kidney was isolated by TRIzol reagent (Thermo Fisher Scientific, Inc.). Next, the RNA integrity of HKT and PKC samples was accurately detected by Agilent 2100 bioanalyzer (Agilent Technologies Inc.). The initial RNA of the library was total RNA, and the total amount was ≥1 μg. The ribosomal RNA in RNA samples was removed to obtain mRNA, and each group of mRNA was randomly cut into fragments and reverse transcribed into cDNA. A 3' adenosine fragment and an Illumina linker (Illumina, Inc.) at the repair end were added to the blunt-ended and phosphorylated cDNA. In order to select cDNA

fragments of preferentially 370-420 bp in length, the library fragments were purified with AMPure XP system (Beckman Coulter, Inc.). The kit used to build the database was the NEBNext® Ultra™ RNA Library Prep Kit (Shanghai Yihui Biological Technology Co., Ltd.) for Illumina. After the construction of the library, the library was initially quantified using a Qubit2.0 Fluorometer (Thermo Fisher Scientific, Inc.), and the library was diluted to 1.5 ng/μl. Next, the insert size of the library was detected using an Agilent 2100 bioanalyzer (Agilent Technologies, Inc.). After the insert size met expectations, the effective concentration of the library was accurately quantified by qRT-PCR (the effective concentration of the library was >2 nM) to ensure the quality of the library. After the library was constructed, it was sequenced by Illumina Novaseq platform (Beijing Novogene Co., Ltd.). Subsequently, the original data were filtered, and the clean reads were quickly and accurately compared with the reference genome (mus_musculus_Ensembl_102, ftp://ftp.ensembl.org/pub/release-102/fasta/mus_musculus/dna/Mus_musculus.GRCm38.dna.toplevel.fa.gz, ftp://ftp.ensembl.org/pub/release-102/gtf/mus_musculus/Mus_musculus.GRCm38.102.gtf.gz) using HISAT2 (version 2.0.5; https://kim-lab.org/) to obtain the positioning information of reads on the reference genome. The percentage of bases with Phred value greater than 20 (Q20) or 30 (Q30) to total bases and GC content of the filtered clean reads were calculated, and all downstream analyses were based on high-quality clean reads. The FeatureCounts tool in the Subread (version 1.3.1; https://bioconductor.org/) was used to measure original gene expression. Sample gene expression was normalized using the gene expression values of all samples reported as fragments per kilobase of transcript per million mapped reads (FPKM) and was successively corrected for sequencing depth and gene length.

Extraction, preparation and analysis of metabolites. After blood collection by laparotomy, the mice were sacrificed, using cervical dislocation as the method of euthanasia. After mice were sacrificed, the kidney tissues of the mice in the PKC and HKT groups were separately isolated, and cold methanol at nine times the volume of the kidney was added. Tissue samples were homogenized on ice with 30-Hz ultrasound for 30 min. After homogenisation, the mixture was shaken for 5 min, centrifuged at 4˚C at 13,400 x g for 15 min (Eppendorf), and the supernatant was transferred to a new centrifuge tube. The remaining precipitate was homogenised again with precooled ethyl acetate:methanol (ratio, 1:3) and centrifuged once under the same conditions. The supernatant obtained from both centrifugation steps was transferred to a fresh glass vial for non-targeted metabolomic analysis. Electrospray ionisation (ESI) was used to detect positive and negative ion patterns. The samples were separated by ultra-high-performance LC and analysed using an Agilent 6550 mass spectrometer (Fig. S1; Agilent Technologies, Inc.). The ESI source conditions were as follows: Gas temperature, 250˚C; dry gas, 16 l/min, atomiser, 20 psig; intrathecal gas temperature, 400˚C; intrathecal gas flow, 12 l/min; Vcap, 3,000 V; nozzle voltage, 0 V; fragment, 175 V; mass range, 50-1,200 m/z; acquisition rate, 4 Hz; cycle time, 250 msec.

Bioinformatics analysis. DESeq2 (version 1.20.0; Bioconductor) (19) was used to analyse DEGs between the HKT and PKC groups, and corrected for P-values (P-adjust). Genes with P-adjust<0.05, and $|\log_2$fold-change(FC)$|\geq 0$ were considered to be DEGs. The screened DEGs were subjected to Gene Set Enrichment Analysis (GSEA; https://www.gsea-msigdb.org/gsea), Gene Ontology (GO; https://www.geneontology.org/) and Kyoto Encyclopaedia of Genes and Genomes (KEGG, https://www.genome.jp/kegg/pathway.html) enrichment analysis. Metabolites with Very Important Pool score (VIP)>1, FC>1.5 or FC>0.667 and P<0.05 were considered to be SDMs taxonomically annotated using the KEGG, Human Metabolome Database (HMDB; https://hmdb.ca/metabolites) and LIPID MAPS (https://lipidmaps.org) databases.

Data collection of IRGs. IRGs were obtained from the Ensembl database (https://www.ensembl.org/). After removing duplicate genes, 689 IRGs were identified (Table SI). When drawing the Venn diagram of DEGs and inflammation-related genes (IRGs), the intersection of the genes in the Venn diagram was defined as the differential IRGs (DE-IRGs). Pearson's correlation coefficients between DE-IRGs and energy metabolism-related genes were calculated using R stats (version 3.6.2; https://rdocumentation.org/packages/stats/versions/3.6.2), and the results are shown as heat maps.

Statistical methods. Data analysis was performed using SPSS (version 18.0; IBM Corp.) and GraphPad Prism (version 8.4.0; GraphPad; Dotmatics). Normality and log normality tests in GraphPad Prism software are used to detect the normality of data. Quantitative data that conformed to a normal distribution are expressed as the mean ± standard deviation of three experiments. All statistical tests in the text are two independent-sample t-tests. P<0.05 was considered to indicate a statistically significant difference. By using the calculation method of linear algebra, the dimensions of tens of thousands of gene variables were reduced and the principal components were extracted, and the gene expression values (FPKM) of all samples were analyzed by PCA. Partial least squares regression was used to establish the relationship model between the expression of metabolites and sample categories, so as to predict the sample categories and establish partial least squares discriminant analysis (PLS-DA) models of each comparison group.

Results

Plateau hypoxia induces kidney injury in mice. Physiological and biochemical changes indicated that the modelling of plateau hypoxia in mice was successful. PaO_2 and SaO_2 in the hypoxic group were significantly decreased by 32.66 and 14.58% (P<0.0001; Table II), respectively. The mRNA and protein expression of *HIF-1α* were upregulated in the kidney tissues of the HKT group compared with that in the PKC group (Fig. 1A-C), suggesting that a plateau hypoxia mouse model was successfully established.

As shown in Table III, compared with that in the PKC group, the body weight of mice decreased significantly after 30 days of plateau hypoxia exposure (HKT group) by 16.28% (P<0.0001). Compared with the PKC group, the kidney mass and index in the HKT group were significantly decreased by 30.41% (P<0.0001) and 17.03% (P<0.01), respectively. This

Table II. Blood gas analysis indexes of two groups of mice.

Blood gas indexes	Groups		
	Plain normoxia	Plateau hypoxia	t
PaO^2, mmHg	94.896±2.592	63.902±3.026	17.4[a]
SaO^2, %	95.006±2.079	81.153±0.961	10.93[a]

Compared with control group, [a]P<0.0001.

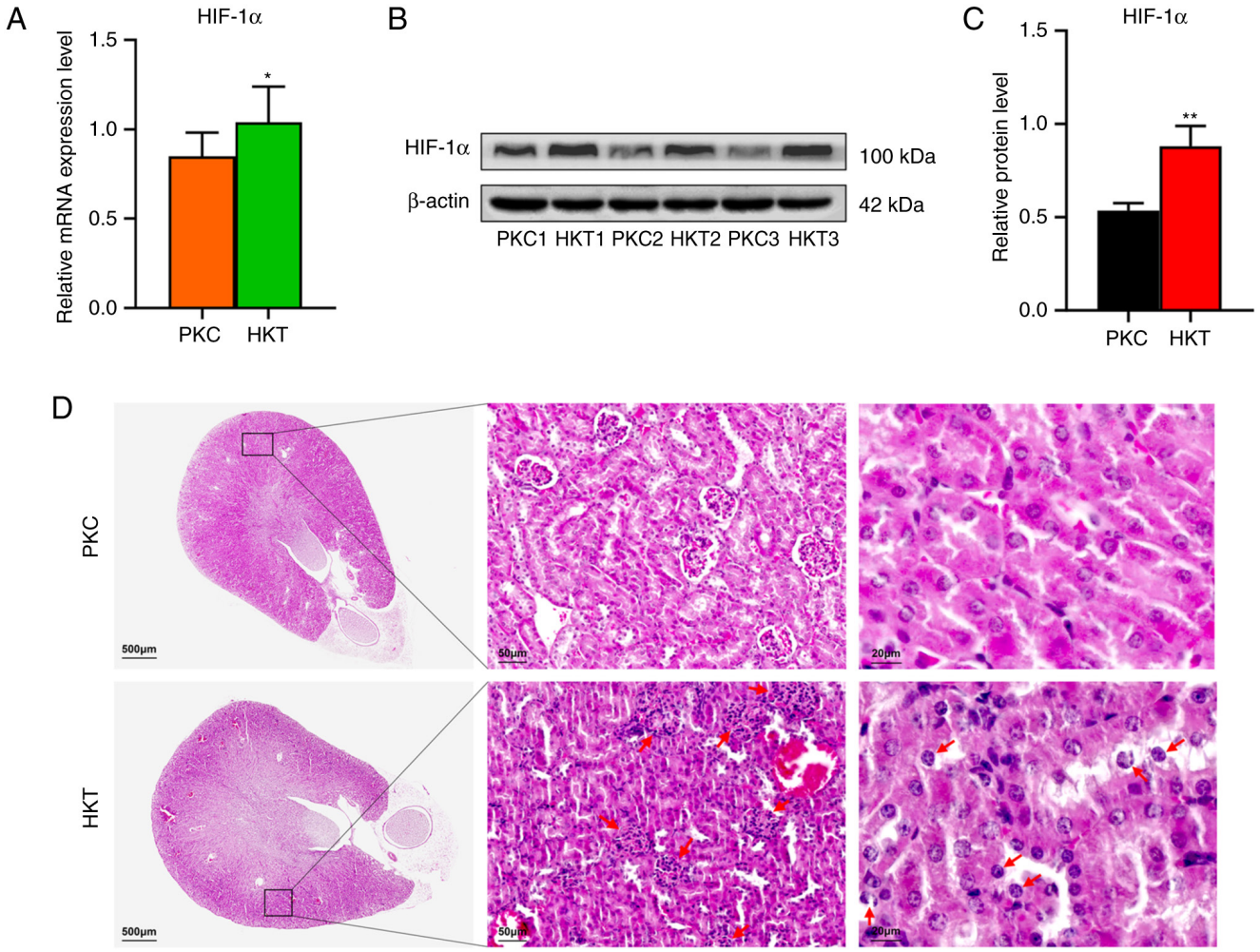

Figure 1. After 30 days of hypoxia treatment, the expression of HIF-1α in the kidney of mice is downregulated and the kidney tissue of mice is damaged. (A) The mRNA expression of HIF-1α. (B) Western blotting of HIF-1α protein expression in the two groups. (C) Quantitative analysis of HIF-1α protein expression, with β-actin as the standard. (D) H&E staining of mouse kidney, with scale bar 500 μm, and the overall morphology of mouse kidney, with scale bar, 50 μm; black box circle area; red arrow refers to atrophic and deformed glomeruli; scale bar, 20 μm. The red arrow pointed to the swelling of renal tubular epithelial cells and cell enucleation. Data are presented as mean ± standard deviation (n=3). Compared with PKC, *P<0.05 and **P<0.01. PKC, plain normoxia group; HKT, plateau hypoxia group.

indicated that kidney weight was reduced in mice under a hypoxic environment in the plateau. In the histological analysis, H&E staining showed that the kidney tissues in the PKC group had normal glomerular and tubular morphology without evident tissue damage. The kidney tissues in the HKT group were damaged, including glomerular atrophy and deformation, irregular arrangement of kidney tubular epithelial cells, swelling of some kidney tubular epithelial cells, erythrocyte exudation and partial cell denucleation (Fig. 1D). It is therefore suggested that hypoxic environment may induce renal tissue damage in mice.

Plateau hypoxia stress alters energy metabolism. The quality of the transcriptome sequencing results was evaluated. The results showed that the PKC and HKT groups achieved clean reads of 41.47 and 40.68 M, respectively. The base error rates

Table III. Kidney indexes of two groups of mice.

Characteristics	Groups		t
	Plain normoxia	Plateau hypoxia	
Body mass, g	22.267±0.619	18.643±0.641	9.097[b]
Bilateral renal mass, g	0.336±0.016	0.234±0.022	8.504[b]
Renal index, %	1.50±0.085	1.27±0.089	4.704[a]

[a]P<0.01 and [b]P<0.0001.

of the data obtained from sequencing, Q20 and Q30 values were 0.02, 98.14 and >94.47%, respectively, and the range of the GC content was 46.97-48.71% (Table SII). The gene expression levels of samples were normalized using FPKM, and the distribution of gene expression levels in different samples was plotted using box-shaped and density diagrams. The results showed that the average Log_2(FPKM+1) values of genes in both the HKT and PKC groups were ~2 (Fig. 2A). The density indices of genes in the PKC and HKT groups were as high as 0.40 and 0.44, respectively (Fig. 2B). PCA results showed that the samples were dispersed among the groups and concentrated within the group (Fig. 2C). Pearson's correlation test showed that the range of inter-sample correlation coefficients (r^2) within the group was 0.811-0.977, with r^2>0.8 (Fig. 2D). These results suggest that the transcriptome sequencing biological experiment was repeatable and that the sequencing data were reliable and could be used for subsequent differential gene analysis.

P-adjust<0.05 and $|\log_2 FC|>0$ were used as the screening thresholds for DEGs. Compared with the PKC group, a total of 3,007 DEGs, 1,349 upregulated and 1,658 downregulated, were identified in the HKT group (Fig. 3A). GSEA was used to enrich all the possible pathways under hypoxic exposure, among which the most significantly enriched gene set was negatively correlated with the hypoxic environment, including Parkinson signalling pathway (Fig. 3B), OXPHOS signalling pathway (Fig. 3C), thermogenic signalling pathway (Fig. 3D), carbon metabolism signalling pathway (Fig. 3E), pyruvate metabolism signalling pathway (Fig. 3F) and TCA cycle signalling pathway (Fig. 3G). The core genes of these pathways were all significantly downregulated (P<0.05).

To further understand the biological functions and adaptive pathways of DEGs under hypoxic stress at the plateau, GO functional annotation and KEGG pathway enrichment analyses were performed on the 3,007 enriched DEGs. GO functional annotation showed that DEGs were enriched in 'biological processes', such as 'ribose phosphate metabolic process', 'purine nucleotide metabolic process' and 'energy production of precursor metabolites'. In terms of 'cellular components', the 'mitochondrial inner membrane', 'organelle inner membrane' and 'mitochondrial protein complex' were the most active. Regarding 'molecular functions', 'structural constituent of ribosome' and 'coenzyme binding' were significantly enriched (Fig. 4A). KEGG pathway enrichment analysis showed that DEGs were significantly enriched in 322 signalling pathways. According to P-adjust, the 20 most significant KEGG pathways were selected to draw the KEGG pathway enrichment map, including those related to energy metabolism, such as 'OXPHOS', the 'TCA cycle', 'peroxisome', 'thermogenesis' and 'carbon metabolism' signalling pathways (Fig. 4B). These results suggest that hypoxic stress at the plateau influences energy metabolism.

TCA cycle and OXPHOS pathways in mouse kidney tissues are inhibited by plateau hypoxia stress. The present study focused on the TCA cycle and OXPHOS signalling pathways under hypoxic conditions. *IDH3A*, *SUCLA2* and *MDH2* are three key enzymes in the TCA cycle for ATP generation, and their downregulation leads to reduced ATP production (20,21). The mRNA expression of genes was examined using RT-qPCR, and the results showed that *IDH3A* (P<0.05), *SUCLA2* (P<0.01) and *MDH2* (P<0.01) were downregulated in the HKT group compared with the PKC group (Figs. 5A and S1A). Accordingly, the protein expression of *IDH3A*, *SUCLA2* and *MDH2* was significantly downregulated in the HKT group compared with that in the PKC group (P<0.05; Fig. 5B and C).

The results of the transcriptome sequencing showed that there were 53 molecular subunits differentially expressed in the mitochondrial electron transport chain (ETC), and the range of $\log_2$FC of these differential molecular subunits was-0.25-3.89 (Table SIII). In the present study, *UQCRC1*, *CYC1*, *UQCRFS1*, *NDUFS7* and *NDUFA3* genes in the OXPHOS pathway were selected for validation using RT-qPCR and western blotting. RT-qPCR results showed that hypoxic exposure significantly reduced the mRNA expression of *UQCRC1* (P<0.05), *CYC1* (P<0.01), *UQCRFS1* (P<0.001), *NDUFS7* (P<0.01) and *NDUFA3* (P<0.001) (Figs. 5D and S1B). Similarly, the protein levels of UQCRC1, CYC1 (P<0.01), UQCRFS1 (P<0.01), NDUFS7 and NDUFA3 (P<0.05) were downregulated in the HKT group, whereas there was no significant downregulation of UQCRC1 and NDUFS7 between the two mouse groups (Fig. 5E and F). These results suggest that hypoxia exposure inhibits the TCA cycle and the OXPHOS signalling pathways (22,23) in mouse kidney tissues (Fig. S2).

Plateau hypoxia stress inhibits energy metabolism. Energy metabolism is the process by which an organism produces ATP via the TCA cycle and OXPHOS (15,16,24). To further investigate whether plateau hypoxia can inhibit energy metabolism in the organism, metabolomic analysis of kidney tissues was

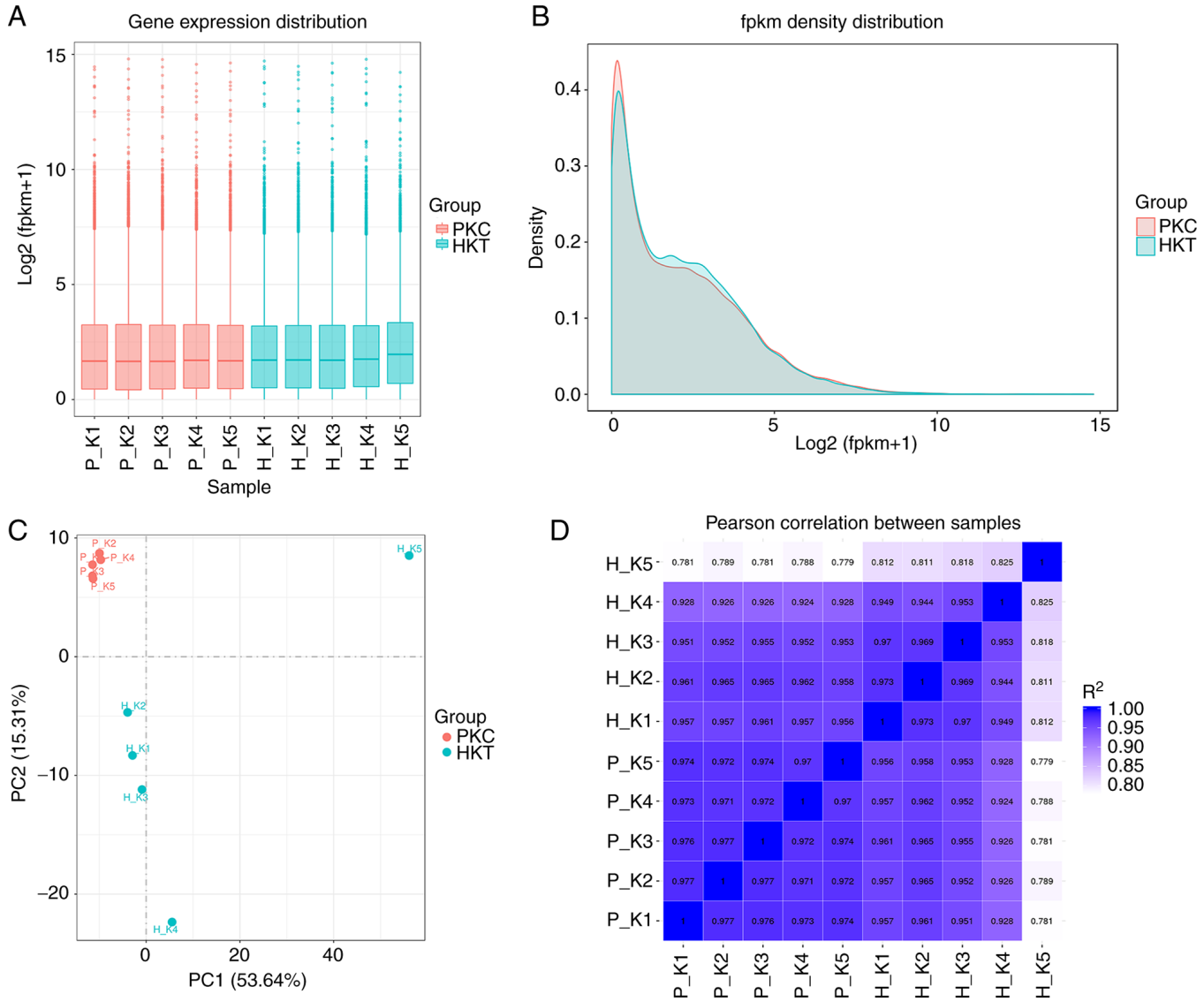

Figure 2. Quality assessment of transcriptome sequencing. (A) Boxplot shows the distribution of gene expression in each sample. (B) Density distribution plot shows the distribution of FPKM within different samples. (C) PC analysis shows the aggregation and separation of samples within and between groups. (D) Pearson's correlation coefficient shows the correlation between different samples, and the horizontal and vertical coordinates in the figure are the squares of the correlation coefficients of each sample. PKC, plain normoxia group; HKT, plateau hypoxia group; PC, principal component; FPKM, Fragments Per Kilobase of transcript per Million mapped reads.

performed to assess changes in differential metabolites associated with energy metabolism induced by hypoxic exposure. Metabolomics PLS-DA score scatter plots (Fig. 6A and B) showed that samples from the HKT and PKC groups were significantly separated in both positive and negative ion modes, with R2Y > Q2Y in both positive and negative ion modes; in the PLS-DA ranking validation plots (Fig. 6C and D), R2 data in positive and negative ionization mode were higher than Q2 data, while the intercept of Q2 regression line and Y-axis were <0. These results indicate that the PLS-DA model has good stability and that there is no overfitting. Hierarchical clustering analysis of the obtained differential metabolites in each group revealed that the metabolic expression patterns in the same comparison group were consistent and the metabolic expression patterns were significantly separated between the two groups (Fig. S3).

When the differential metabolites detected in the positive and negative ion models were combined, 365 SDMs (P<0.05) were detected between the HKT and PKC groups (VIP>1; P<0.05; Fig. 7A), of which 190 and 175 were significantly upregulated and downregulated, respectively. In addition, KEGG results revealed that SDMs were mainly enriched in metabolic processes, such as 'energy metabolism', 'nucleotide metabolism', 'amino acid metabolism', 'metabolism of cofactors and vitamins', 'lipid metabolism' and 'carbohydrate metabolism' (Fig. 7B). SDMs were primarily annotated in the HMDB database with 'organic acids and derivatives', and 'lipids and lipid-like molecules' (Fig. S4). The results annotated by Lipid MAPS show that SDMs are mainly enriched in 'fatty acids and conjugates', 'eicosanoids', 'fatty esters' of fatty acyls, glycosides in glycerophospholipids and 'flavonoids' of polyketides (Fig. S5).

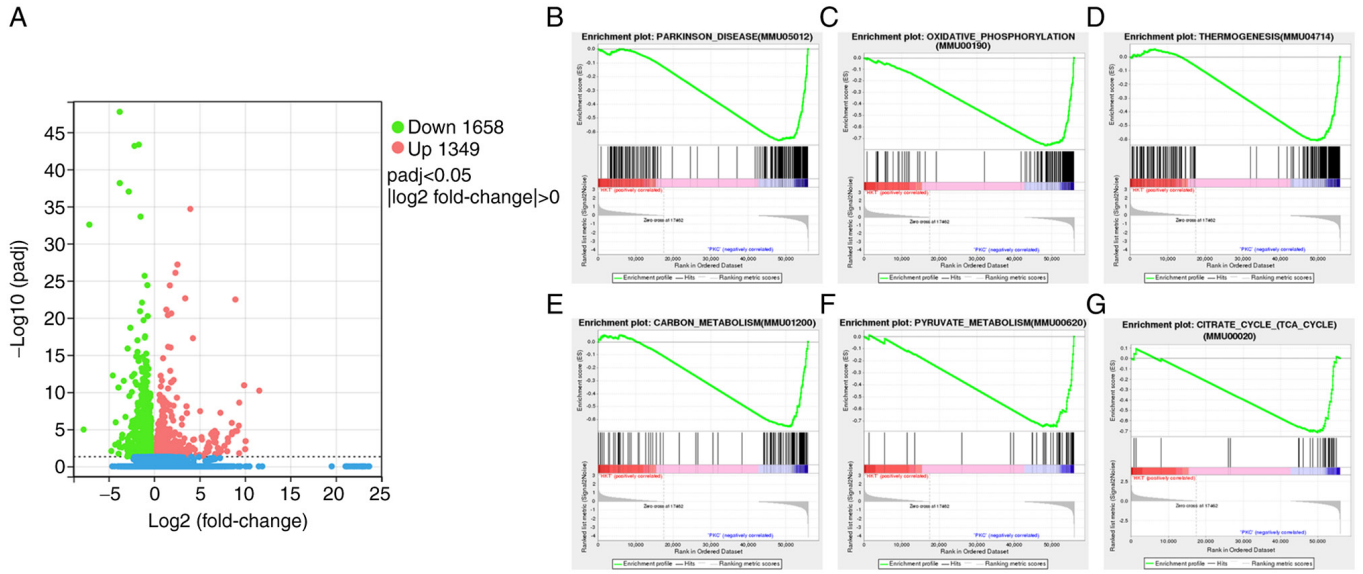

Figure 3. A total of 3,007 DEGs are enriched under hypoxia exposure. (A) Volcano map of DEGs, 1,349 and 1,658 genes were upregulated and downregulated, respectively. (B-G) Gene set enrichment analysis of the transcriptome. DEGs, differentially expressed genes.

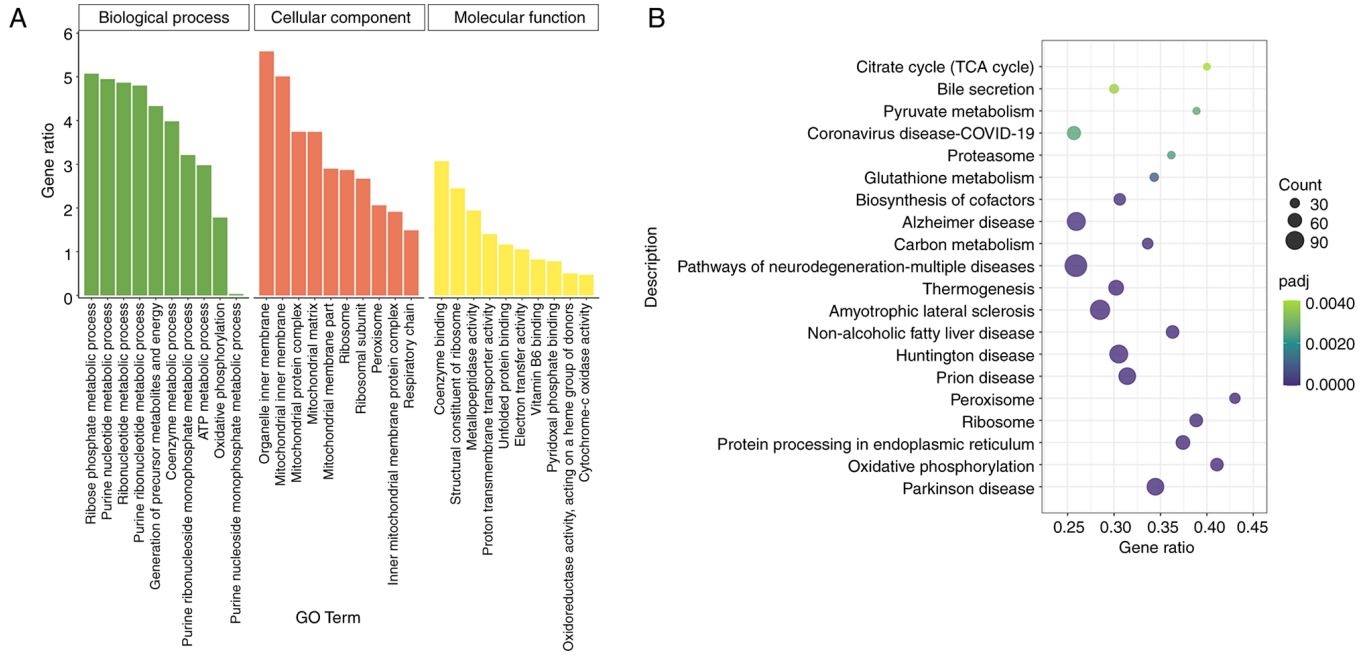

Figure 4. DEGs mainly enriche the pathway of energy metabolism after treatment for 30 days in a hypoxic environment. (A) GO enrichment analysis of DEGs. (B) KEGG enrichment analysis map of DEGs. GO, gene ontology; DEGs, differentially expressed genes; KEGG, Kyoto Encyclopedia of Genes and Genomes; TCA, tricarboxylic acid.

The metabolomic results showed that most amino acids in the kidney tissues of mice in the HKT group were significantly downregulated compared with those in the PKC group, with L-hydroxylysine and L-cysteine significantly decreased by 86.48% (P<0.001) and 76.21% (P<0.05), respectively (Fig. 8A). In addition, Asp-Phe, N-acetyl-L-leucine, S-adenosyl-L-methionine, N-acetyl valine, N-acetyl glycine and 5-oxoproline levels decreased by >41.44% compared with those in the PKC group (Table SIV). Among these significantly decreased amino acids, some participate in the central carbon metabolism of the organism and thus in the TCA cycle (Fig. 8D). Further analysis of the metabolomic data revealed that cis-aconitic acid and α-ketoglutarate, which are involved in the TCA cycle, were significantly reduced by 67.98% (P<0.001) and 78.11% (P<0.05), respectively, under high-altitude hypoxia exposure (Fig. 8B). The pentose phosphate pathway is a mode of glucose oxidative decomposition that provides multiple raw materials for the synthesis and metabolism of purines and pyrimidines (Fig. 8D). NADPH is mainly generated via the pentose phosphate pathway. Although NADPH cannot directly enter the respiratory linkage to be oxidised, the H^+ in NADPH can be

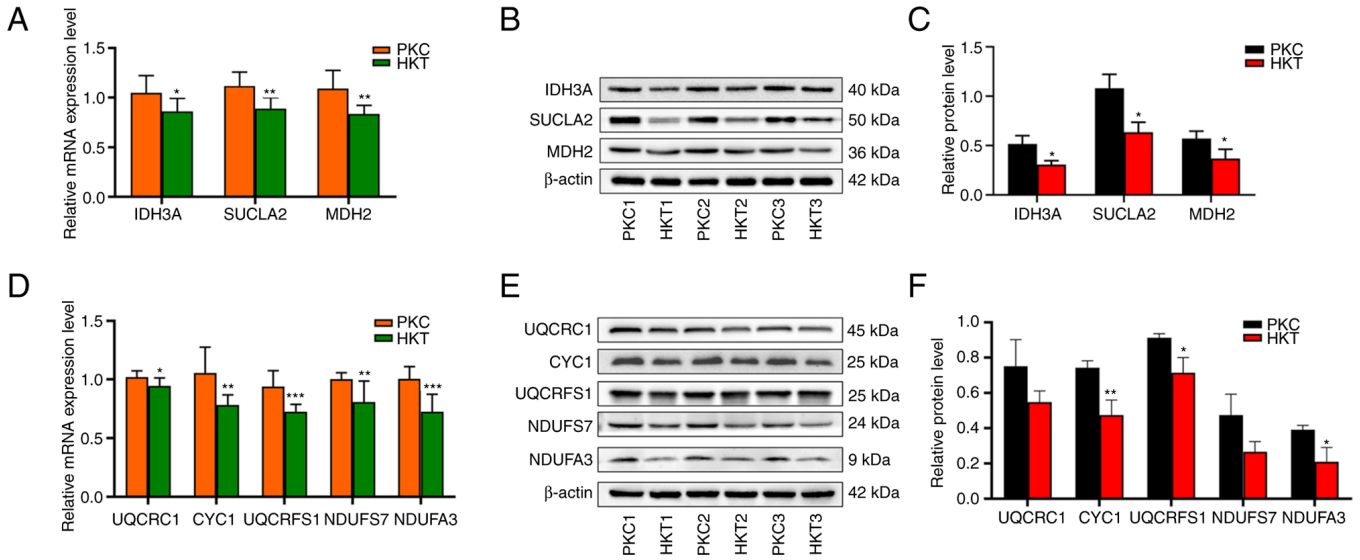

Figure 5. After 30 days of hypoxia treatment, the expression levels of key genes and their encoded proteins in the TCA cycle and OXPHOS pathways are downregulated. (A) mRNA expression, (B) protein expression and (C) protein quantification of *IDH3A*, *SUCLA2* and *MDH2* genes in the TCA cycle pathway, with β-actin as the standard. (D) mRNA expression, (E) protein expression and (F) protein quantification of *UQCRC1, CYC1, UQCRFS1, NDUFS7* and *NDUFA3* genes in the OXPHOS pathway, with β-actin as the standard. Compared with the PKC group, *P<0.05, **P<0.01 and ***P<0.001 (n=3). PKC, plain normoxia group; HKT, plateau hypoxia group; OXPHOS, oxidative phosphorylation; TCA, tricarboxylic acid.

transferred to NAD^+ and converted to NADH to enter the electron transport chain to participate in ATP production. In the current study, NADPH and NADH levels in the HKT group were significantly decreased by 63.92 and 74.87% (P<0.01 for both), respectively compared with those in the PKC group (Fig. 8C). These results indicated that hypoxia exposure inhibits the central hubs of the three major energy metabolism pathways and suppresses the synthesis of amino acids and the upstream products of the mitochondrial electron transport chain.

After 30 days of hypoxic exposure, the metabolism of purine and pyrimidine in the kidney tissues of the mice changed (Fig. 9A). In purine metabolism, the concentrations of GDP, GMP, guanine, ADP, adenine, deoxyadenosine and xanthosine monophosphate (XMP) were downregulated in the kidney tissues of mice in the HKT group compared with those in the PKC group, with a significant decrease of >41.86% (P<0.05) in adenine, deoxyadenosine and XMP (Fig. 9B; Table SV). In terms of pyrimidine metabolism, the concentrations of dCDP, thymidine, thymine, UDP, UMP, CTP and CDP were downregulated in the kidney tissues of mice in the HKT group, among which the concentrations of thymidine, thymine, and UDP were significantly downregulated by 44.59% (P<0.01), 44.03% (P<0.05) and 69.31% (P<0.01), respectively (Fig. 9B; Table SV). These results suggest that exposure to hypoxia disrupts nucleotide synthesis. To assess the consistency of metabolite and metabolite trends, Pearson's correlation coefficient of metabolites involved in amino and nucleotide synthesis revealed that the correlations were all positive (Fig. S6). The aforementioned results further show that the energy metabolism of mouse kidney tissue is inhibited in a hypoxic environment.

Hypoxia exposure induces inflammatory reactions in histiocytes. Impaired energy metabolism leads to decreased production of adenosine triphosphate and increased production of free radicals, exacerbating the inflammatory response (25). To further explore the mechanism of inflammatory reactions induced by hypoxia exposure in mouse kidney tissues, a cross-analysis was conducted between DEGs and IRGs, indicating that 113 genes were DE-IRGs (Fig. 10A). A total of eight DEGs in the TCA cycle and the OXPHOS signalling pathways were defined as energy metabolism-related differential genes (ER-DEGs). Results showed that the correlation between DE-IRGs and ER-DEGs was either positive or negative, and there were more negatively than positively correlated genes (Fig. 10B). The mRNA and protein expression levels of the DEGs *IL1B*, *IL12B*, *S100A8* and *S100A9* were subsequently verified by RT-qPCR and western blotting. The results showed that the mRNA and protein expression of *IL1B*, *IL12B* and *S100A9* were significantly upregulated (P<0.05). The mRNA expression of *S100A8* was significantly upregulated (P<0.0001); however, its protein expression was not significantly different (Fig. 10D-F). Pearson's correlation coefficients of inflammatory factors *IL1B*, *IL12B*, *S100A8* and *S100A9* with ER-DEGs revealed negative correlations (Fig. 10C), indicating that downregulated expression of ER-DEGs promoted the expression of the inflammatory factors *IL1B*, *IL12B*, *S100A8* and *S100A9,* and induced an inflammatory response. These results further suggest that energy metabolism inhibition influences inflammation in the kidney tissues of mice.

Discussion

In the current study, C57BL/6 mice were maintained at an altitude of 4,200 m in Maduo, China to construct a plateau hypoxia animal model. Transcriptomic sequencing and non-targeted metabolomics were used to detect and analyse DEGs and SDMs in the kidneys of PKC and HKT mice. The mechanism by which hypoxia inhibits energy metabolism and leads to

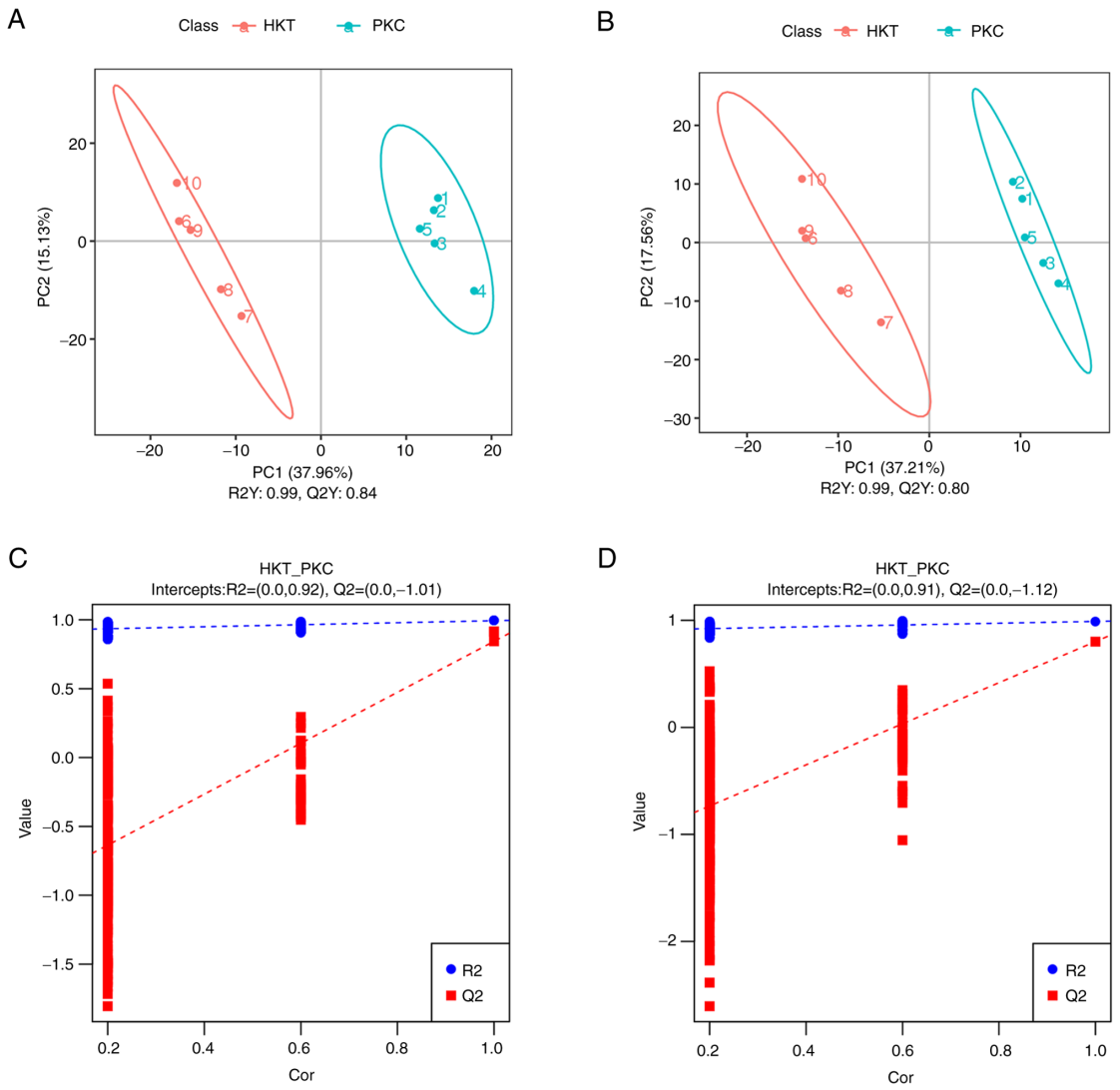

Figure 6. Renal metabolomics data of C57BL/6 mice exposed to hypoxia compared with the PKC group are reliable. (A and B) Scatter plots of metabolomics PLS-DA scores and (C and D) the validation plots of PLS-DA ordering for the control group and the hypoxic treatment group were used to evaluate the stability of the model. (A) and (C) from positive ionization mode. (B) and (D) from self-ionization mode. Cor, correlation; PKC, plain normoxia group; HKT, plateau hypoxia group; PLS-DA, partial least squares discriminant analysis.

kidney inflammation in mice was investigated. Under normoxic conditions, *HIF-1α* is degraded by prolyl hydroxylase, which uses oxygen as a substrate. Therefore, hypoxia inhibits HIF-1α prolyl hydroxylation and upregulates the expression of *HIF-1α*, which regulates adaptation to hypoxic environments (26). In the current study, the mRNA and protein expression levels of *HIF-1α* in the HKT group were significantly upregulated compared with those in the PKC group, indicating that the hypoxic animal model was successfully established. Changes in body mass and organ index are important health indicators. Therefore, the kidney and body mass of mice were further measured, and it was found that they were both significantly decreased, and the kidney index was also decreased. H&E staining results showed that the HKT group displayed obvious kidney damage, including glomerular atrophy and deformation, irregular arrangement of tubular epithelial cells, swelling of some tubular epithelial cells, exudation of erythrocytes and denucleation of some cells compared with the PKC group. These results suggest that exposure to hypoxia leads to significant changes in the kidney tissues of mice.

To clarify the key pathways and genes that induce alterations in the kidney under hypoxic stimulation, DEGs were enriched for KEGG pathways and KEGG results of mouse kidney tissue transcriptomic analysis showed that metabolism-related pathways, such as 'OXPHOS', 'TCA cycle', 'peroxisome', 'thermogenesis' and 'carbon' metabolism signalling pathways, were significantly enriched. Energy metabolism is the process of generating ATP through OXPHOS and the TCA cycle. Therefore, the mechanism of hypoxic exposure on the TCA cycle and OXPHOS signalling pathways was further investigated. A previous study showed that *IDH3* is an NAD^+-dependent heterotetrameric enzyme that irreversibly catalyses the conversion of isocitrate (ICT) to α-ketoglutarate (AKG) (27). The conversion of ICT to AKG is necessary for the TCA cycle and the production of NADH during OXPHOS for ATP generation (28). Succinyl coenzyme A synthase (SCS) is a TCA cycle enzyme responsible for the conversion of succinyl coenzyme A to succinic acid in the mitochondrial matrix and is coupled with phosphorylation of GDP or ADP, thus providing the only 'substrate level' phosphorylation in the TCA cycle (29).

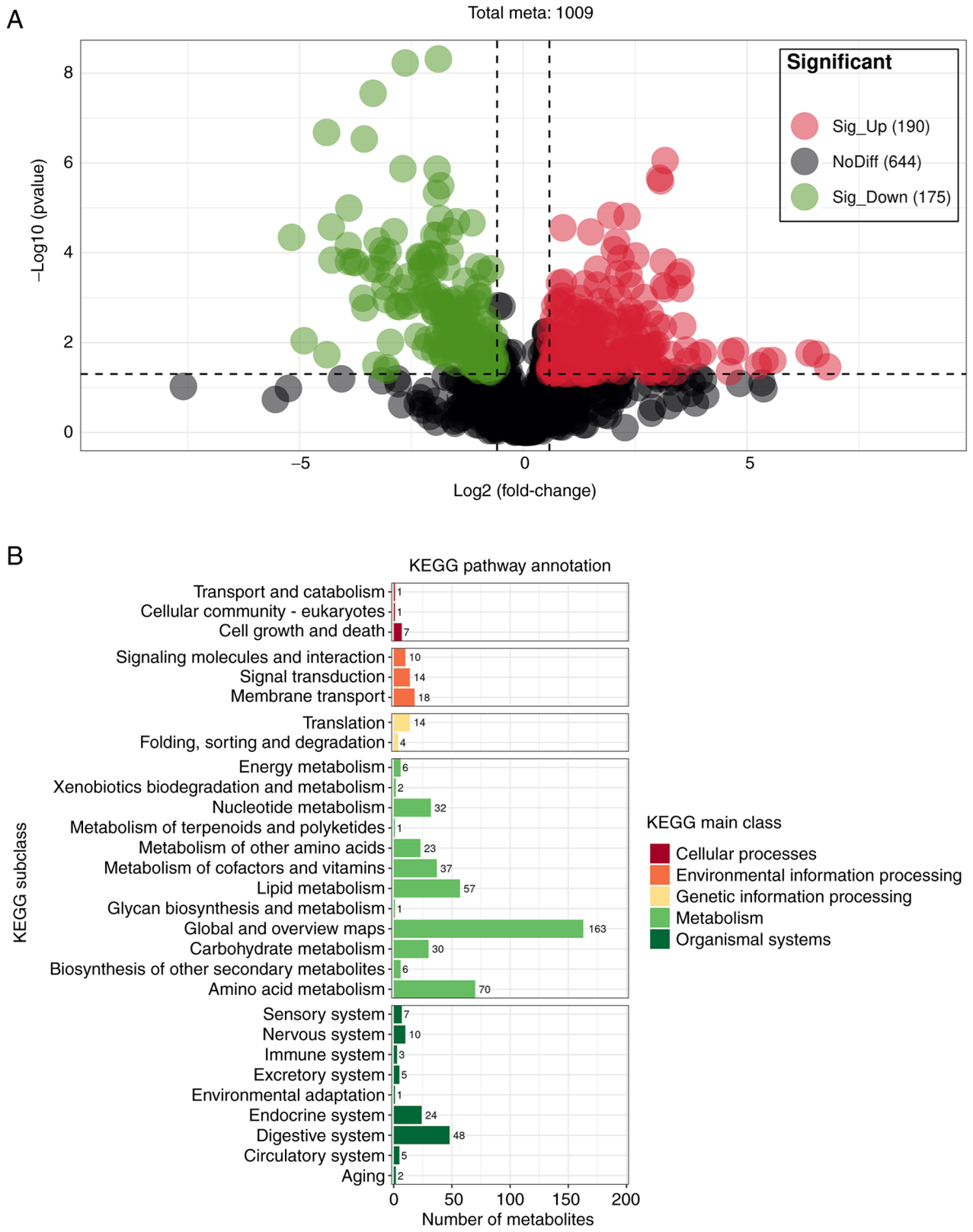

Figure 7. A total of 365 SDMs were detected between the HKT and PKC groups, and SDMs are mainly enriched in energy metabolism pathway. (A) Volcanic diagram showing the expression of SDMs in mouse kidney tissue under hypoxic exposure. The gray dotted line in the diagram represented the threshold line of SDMs screening criteria, and the red, green and black circles respectively represented the metabolites significantly upregulated, significantly downregulated and without difference. (B) KEGG enrichment profile for SDMs. SDMs, significantly different metabolites; KEGG, Kyoto Encyclopaedia of Genes and Genomes; PKC, plain normoxia group; HKT, plateau hypoxia group.

SUCLA2 encodes an ADP-specific β-subunit subtype of SCS (30) and its downregulation inhibits mitochondrial respiratory activity (31). Malate dehydrogenase 2 (MDH2) catalyses the reversible reduction of oxaloacetate to l-malate

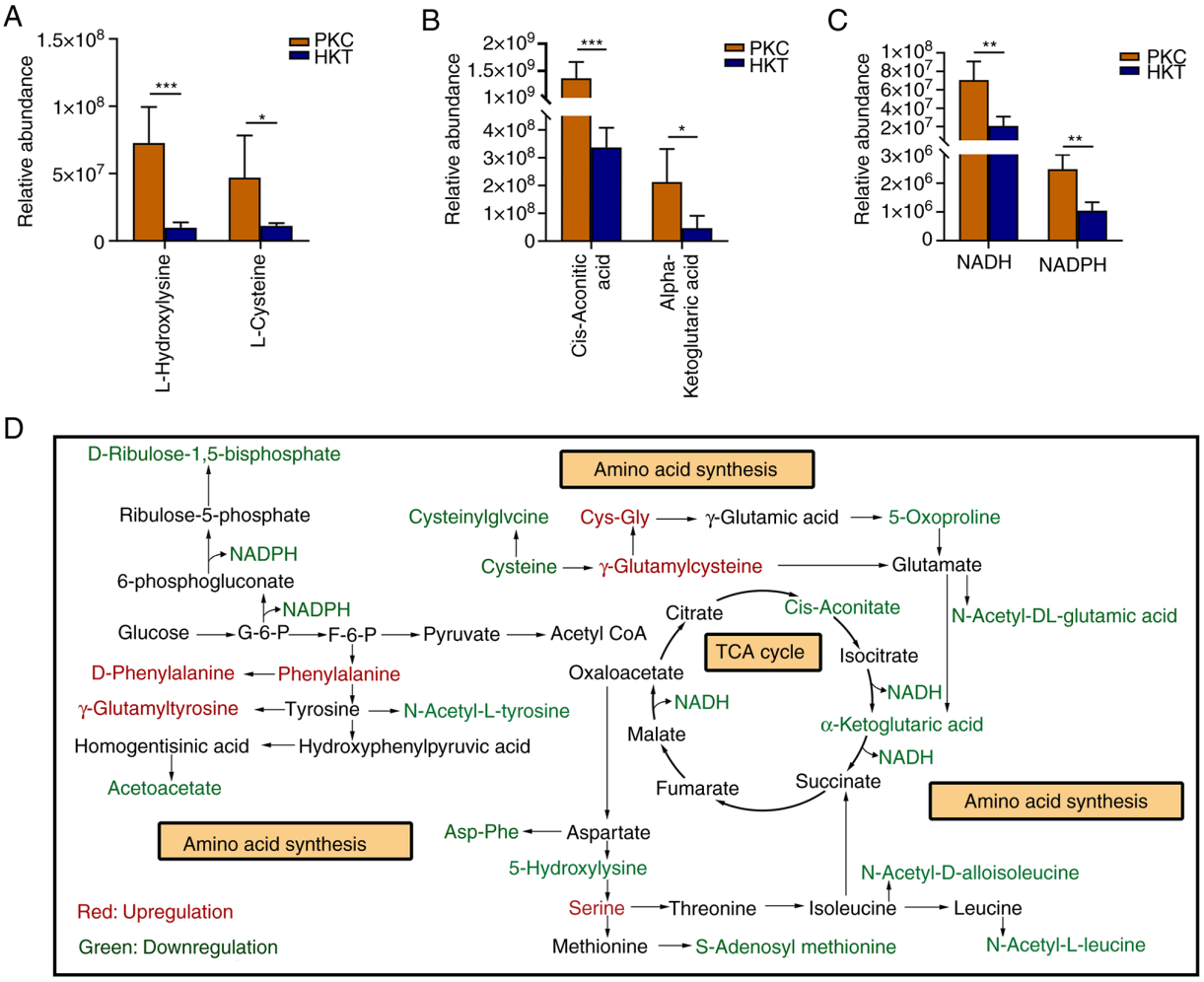

Figure 8. After 30 days of hypoxic exposure, compared with the PKC group, the energy metabolism and amino acid synthesis in the kidney tissue of the HKT group is disordered. (A) Downregulation of concentration of L-hydroxylysine and L-cysteine in HKT group. (B) Downregulation of concentration of cis-aconitic acid and α-ketoglutaric acid in the HKT groups. (C) Downregulation of concentration of NADH and NADPH in the hypoxia treatment group. (D) The most relevant metabolites the are disrupted by hypoxic exposure in central carbon metabolism and amino acid synthesis, in which hypoxia exposure inhibits amino acid synthesis and central carbon metabolism. Data are expressed as mean ± standard deviation (n=3). Compared with the PKC group, *P<0.05, **P<0.01 and ***P<0.001. PKC, plain normoxia group; HKT, plateau hypoxia group.

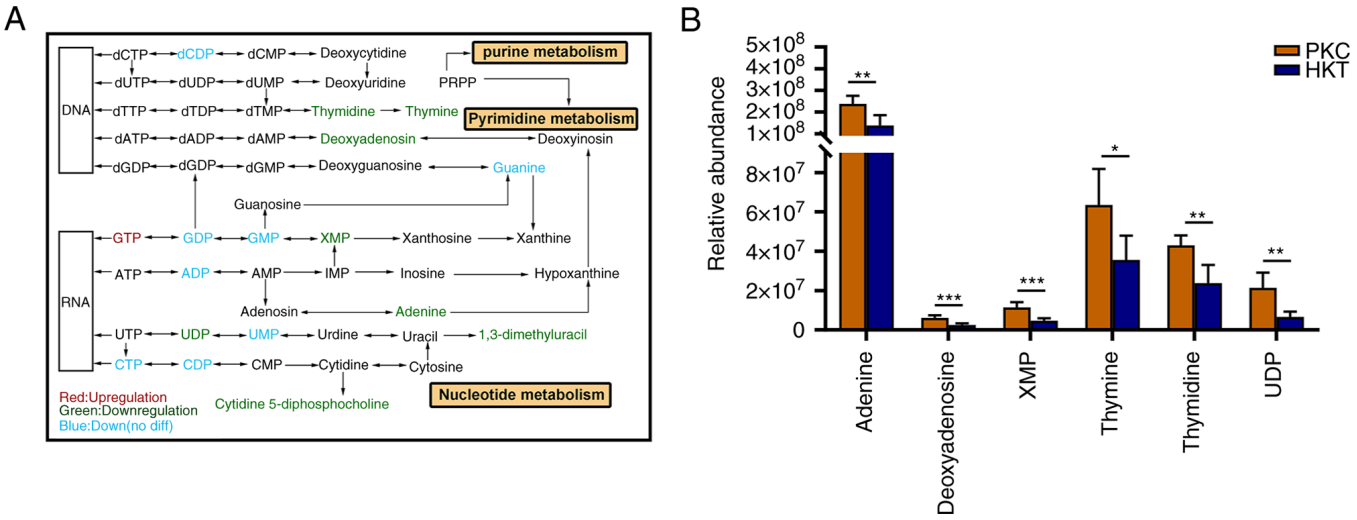

Figure 9. After 30 days of hypoxic exposure, compared with the PKC group, the nucleotide metabolism in the kidney tissue of the HKT group is disordered. (A) The most relevant metabolites that are disrupted by hypoxic exposure in purine and pyrimidine metabolism, in which hypoxia exposure inhibits nucleotide synthesis. (B) Downregulation of concentration of adenine, deoxyadenosine, XMP, thymidine, thymine and UDP in the kidney of mice in the hypoxia treatment group. Data are expressed as mean ± standard deviation (n=3). Compared with the PKC group, *P<0.05, **P<0.01 and ***P<0.001. PKC, plain normoxia group; HKT, plateau hypoxia group.

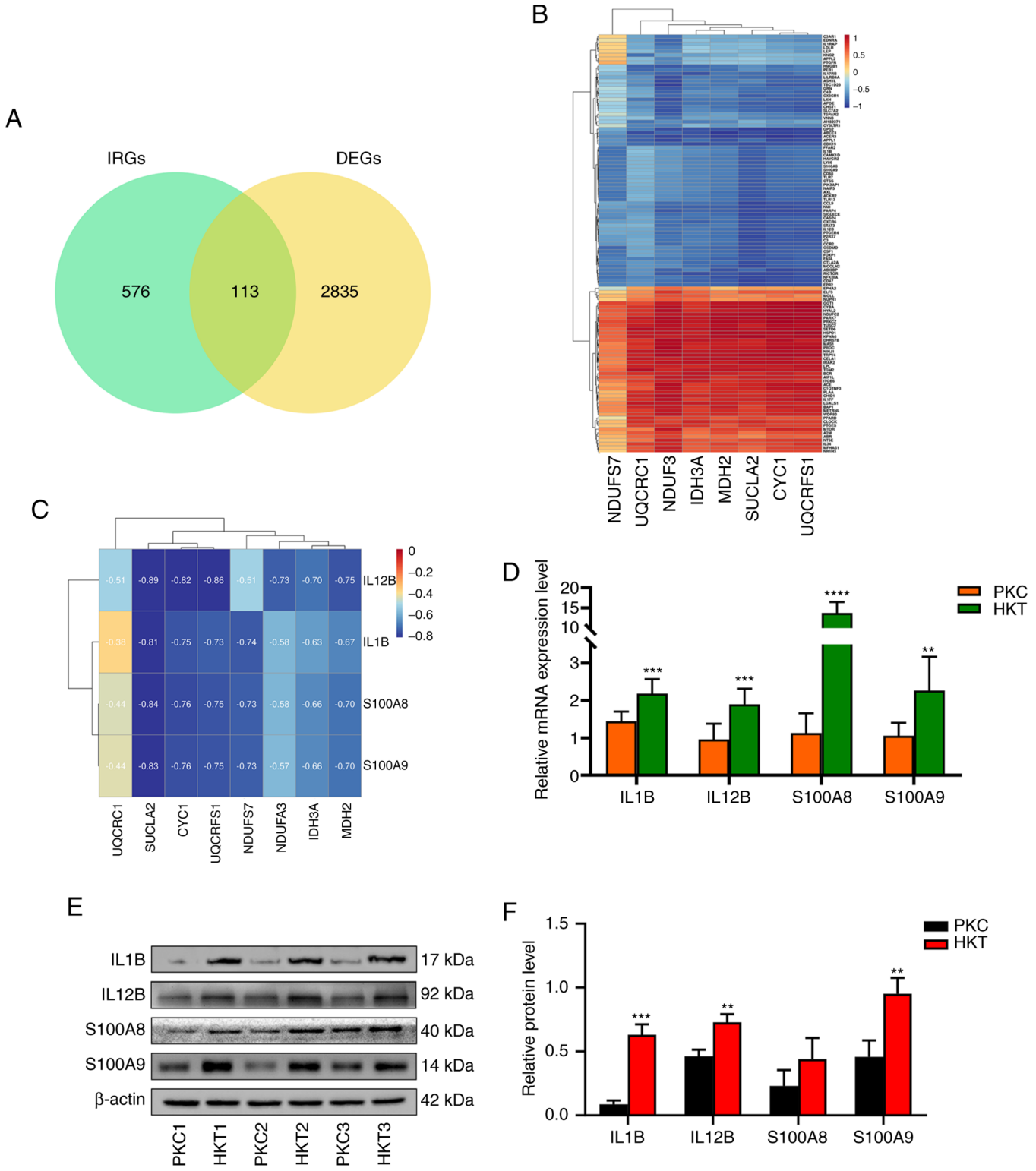

Figure 10. Correlation analysis of ER-DEGs and inflammatory factors and expression of inflammatory factors. (A) Venn diagram of DE-IRGs and a total of 113 DE-IRGs were identified; (B) Correlation analysis between ER-DEGs and DE-IRGs, there is a positive or negative correlation between ER-DEGs and DE-IRGs; (C) The correlation analysis between ER-DEGs and inflammatory factors IL1B, IL12B, S100A8 and S100A9 was negatively correlated. (D) mRNA expression, (E) protein expression and (F) protein quantification of inflammatory factors IL1B, IL12B, S100A8 and S100A9 genes were upregulated, with β-actin as the standard. Data were expressed as mean ± standard deviation (n=3). Compared with the PKC group, **P<0.01, ***P<0.001 and ****P<0.0001. PKC, plain normoxia group; HKT, plateau hypoxia group; DE-IRGs, differential inflammation-related genes; ER-DEGs, energy metabolism-related differential genes.

depending on NAD$^+$ (32). MDH2 deficiency limits the flux of pyruvate to complex I of the mitochondrial electron transport chain, thereby reducing complex I-dependent respiration (33). By contrast, MDH2 deficiency interrupts the TCA cycle and mitochondrial NADH levels, resulting in an inadequate energy supply (34). In the present study, hypoxic exposure

significantly reduced the mRNA and protein expression of *IDH3A*, *SUCLA2* and *MDH2* in the TCA cycle. It is suggested that the hypoxic plateau environment inhibits the TCA cycle and suppresses ATP production in the mouse kidney.

The OXPHOS system of the mitochondrial inner membrane consists of five enzymes [complexes I-V (cI-V)] (35,36), and the RNA-seq results showed that several molecular subunits in cI and cIII in the mitochondrial ETC were significantly downregulated under hypoxic exposure, suggesting that hypoxic stress may lead to changes in mitochondrial function. Mitochondrial respiratory chain complex I (cI, NADH-ubiquinone reductase/NADH dehydrogenase) is the main entrance of the mitochondrial respiratory chain, which accepts the electron transfer of NADH to ubiquinone and couples with the proton pump, thus providing proton power to ATP synthase for the production of ATP (36,37). cI is the largest ETC enzyme and consists of 45 subunits (38). *NDUFA3* is required for the assembly and/or stabilisation of the cI matrix arm in human mitochondria, and *NDUFA3* is necessary for the formation of functional cI (39). *NDUFS7* is one of the subunits of iron-sulphur proteins in cI, which is involved in the transfer of electrons in the respiratory chain and is the catalytic centre of electron flow in cI (40). *NDUFS7* subunits are essential for maintaining cI activity, and their degradation leads to a decrease in cI activity (41). The data of the current study showed that *NDUFA3* and *NDUFS7* are downregulated in mouse kidney tissues exposed to hypoxic conditions, indicating that exposure of the organism to chronic hypoxia leads to decreased stability and activity of cI, which inhibits the function of the mitochondrial ETC and energy production.

In the current study, it was found that hypoxia exposure downregulated the mRNA and protein expression of *UQCRC1*, *CYC1* and *UQCRFS1* subunits in cIII. The assembly of 10 subunits encoded by nuclear DNA and one subunit encoded by mitochondrial DNA generates functional cIII, which transfers electrons from ubiquinol to cytochrome c (42). UQCRFS1 is a protein containing the Fe/S cluster, which is the last component inserted into cIII. The insertion of *UQCRFS1* is essential for the stable formation of cIII (43), while its mutation is a causative factor of cIII deficiency (44). *UQCRC1* is a key component of cIII in the mitochondrial respiratory chain. *UQCRFS1* is notably upregulated in *UQCRC1*-overexpressing cells. *UQCRC1* overexpression leads to increased mitochondrial OXPHOS and ATP production (45). Downregulation of *UQCRC1* promotes mitochondrial membrane potential collapse by increasing ROS production, thereby impairing mitochondrial function and affecting energy metabolism (46). Dysfunction of *UQCRC1* and *UQCRFS1* is associated with reduced cIII and brain mitochondrial content (47). In addition, *CYC1* is one of the component subunits of mitochondrial cIII. Downregulation of *CYC1* decreases mitochondrial cIII activity and increases the ratio of AMP to ATP (48). Based on these findings, it is suggested that hypoxia exposure disrupts mitochondrial function and inhibits energy metabolism.

To further confirm that hypoxic exposure inhibits energy metabolism, we performed a non-targeted metabolomic analysis of the kidney. A total of 365 SDMs were identified by non-targeted metabolomics in positive and negative ion modes. KEGG results showed that SDMs were mainly enriched in metabolic processes, such as 'energy metabolism', 'nucleotide metabolism', 'amino acid metabolism', 'cofactor and vitamin metabolism', 'lipid metabolism' and 'carbohydrate metabolism'. This indicates that plateau hypoxic stress alters energy metabolism. Cis-aconitate and α-ketoglutarate are key intermediate metabolites of the TCA cycle. In the present study, hypoxic exposure reduced the concentrations of cis-aconitic acid and α-ketoglutarate, confirming that hypoxic stress inhibits the TCA cycle. Inhibition of the TCA cycle inevitably reduces the efficiency of electron transfer to ubiquinone, thereby inhibiting the energy metabolism of OXPHOS. NADH and NADPH are involved in numerous biological reactions as electron carriers (49). NADH is mainly involved in energy metabolism through glycolysis and OXPHOS for ATP production, whereas NADPH is used to maintain redox homeostasis and nucleotide biosynthesis (50,51). The results of the present study showed that the concentrations of NADH and NADPH in the HKT group were significantly lower than those in the PKC group, indicating that hypoxic exposure inhibited the electron transfer process of OXPHOS and suppressed energy metabolism. Due to this inhibition of energy metabolism, the synthesis of amino acids, nucleotides, and other nutrients is bound to decrease, which may inhibit various biological reactions and ultimately affect cell growth (52). In the current study, the concentrations of most amino acids, pyrimidines and purines in the kidney tissues of mice were significantly downregulated under hypoxic exposure.

Inhibition of energy metabolism can lead to inflammation. cI and III are generally considered the main sites of ROS production (53). Impaired mitochondrial respiratory chain complexes may lead to reduced ATP synthesis and increased ROS production (54), which increases the inflammatory response (55). Therefore, to further investigate the mechanism of the inflammatory response caused by the inhibition of energy metabolism, 113 DE-IRGs were identified by analysing the inflammatory response database. It was found that the correlation between DE-IRGs and ER-DEGs was either positive or negative, and the number of negatively correlated genes was greater than that of positively correlated genes. These results suggest that ER-DEG may play a role in the development of renal inflammatory response stimulated by hypoxia. A previous study showed that *IDH1* and *IDH2* mRNA expression is notably reduced in the skin surrounding hidradenitis suppurativa lesions (56). Deletion of *SUCLA2* leads to TCA circulatory failure, mitochondrial DNA depletion and fatal childhood encephalomyopathy (57). In addition, *MDH2* silencing promotes ovarian cancer cell proliferation *in vitro* and *in vivo* (58). Microglia U90926 directly binds to *MDH2* and competitively reduces *MDH2*-mediated *CXCL2* mRNA degradation, thereby promoting neutrophil infiltration (59). *NDUFA3* and *NDUFS7* may play important roles in regulating oxidative stress, apoptosis, and inflammatory responses during cerebral ischaemia-reperfusion (60). Based on the aforementioned results, the mRNA and protein expression of the inflammatory factors *IL1B*, *IL12B*, *S100A8* and *S100A9* was verified. The results showed that *IL1B*, *IL12B*, *S100A8* and *S100A9* were upregulated. It has been suggested that inhibition of energy metabolism induces inflammation.

The present study provides convincing evidence that hypoxia exposure inhibits energy metabolism by suppressing the TCA cycle and OXPHOS pathway, leading to amino acid and nucleotide deficiencies, and further inducing

inflammation. The current study has several advantages, despite only reporting preliminary data. In animal experiments, mice were placed in a highland area at an altitude of 4,200 m to establish animal models to simulate human exposure in the real world. In addition, the present study applied multi-omics techniques to comprehensively evaluate biological changes in the mouse kidney under hypoxic exposure. Transcriptomic results showed that hypoxic exposure inhibited the TCA cycle and OXPHOS pathway in the kidney. Non-targeted metabolomics confirmed that hypoxic exposure inhibited energy metabolism, resulting in a lack of amino acids and nucleotides. By associating DEGs with the inflammatory response database, it was found that hypoxic exposure could induce inflammation. At present, for the treatment of chronic hypoxia, HIF oxygen-dependent prolyl hydroxylase inhibitor, sodium-glucose cotransporter 2 inhibitor, antioxidant drugs melatonin and hydrogen sulphide are mainly used to improve hypoxia-induced renal inflammation (61). However, the present study has some limitations. It is difficult to establish a high altitude hypoxia model, and the sample size is small, hence periodic acid-Schiff, periodic acid-silver metheramine and immunohistochemical staining were not used in the early experimental design of the present study to measure the glomerular injury score and the number of tubular necrosis. In addition, there is no direct evaluation of the relationship between metabolites involved in amino acid and nucleotide synthesis and inflammatory reaction. Moreover, the conclusions would be more convincing if the genes related to energy metabolism, which are altered under hypoxic conditions, were induced to be expressed at high levels or knocked out. The current study provides new insights into hypoxia-mediated kidney injury, which will guide future studies about the specific mechanism through which hypoxia inhibits energy metabolism and induces inflammation.

Acknowledgements

Not applicable.

Funding

The present study was funded by National Natural Science Foundation of China (grant no. 82060295) and by the Applied Basic Research Project of Qinghai Province (grant no. 2023-ZJ-771).

Availability of data and materials

The datasets used and/or analyzed during the current study are available from the corresponding author on reasonable request. The Illumina sequencing data were deposited in the Gene Expression Omnibus database (accession no. GSE240049; https://www.ncbi.nlm.nih.gov/geo/query/acc.cgi?acc=GSE240049).

Authors' contributions

YG carried out the experimental work and wrote the manuscript. QL designed the experiments. HY carried out transcriptomics sequencing. YH assisted with transcript expression assessments. YX performed metabolomics data analysis. CT analyzed the data of RT-qPCR. CG analyzed the western blotting data. SY established animal models of hypoxia and normoxicity. YG and SY confirm the authenticity of all the raw data. All authors read and approved the final version of the manuscript.

Ethics approval and consent to participate

Animal experiments were approved by the Animal Ethics Review Committee of Medical College of Qinghai University (approval no. 2020-005) and all procedures were carried out in accordance with the guidelines for the care and use of experimental animals of the National Institutes of Health.

Patient consent for publication

Not applicable.

Competing interests

The authors declare that they have no competing interests.

References

1. Li Y, Zhang Y and Zhang Y: Research advances in pathogenesis and prophylactic measures of acute high altitude illness. Respir Med 145: 145-152, 2018.
2. Gaur P, Prasad S, Kumar B, Sharma SK and Vats P: High-altitude hypoxia induced reactive oxygen species generation, signaling, and mitigation approaches. Int J Biometeorol 65: 601-615, 2021.
3. Yang S and Lian G: ROS and diseases: Role in metabolism and energy supply. Mol Cell Biochem 467: 1-12, 2020.
4. Wilkins MR, Ghofrani HA, Weissmann N, Aldashev A and Zhao L: Pathophysiology and treatment of high-altitude pulmonary vascular disease. Circulation 131: 582-590, 2015.
5. Clark AJ and Parikh SM: Mitochondrial metabolism in acute kidney injury. Semin Nephrol 40: 101-113, 2020.
6. Infantino V, Santarsiero A, Convertini P, Todisco S and Iacobazzi V: Cancer cell metabolism in hypoxia: Role of HIF-1 as key regulator and therapeutic target. Int J Mol Sci 22: 5703, 2021.
7. Fuhrmann DC and Brüne B: Mitochondrial composition and function under the control of hypoxia. Redox Biol 12: 208-215, 2017.
8. Liu X, Du H, Sun Y and Shao L: Role of abnormal energy metabolism in the progression of chronic kidney disease and drug intervention. Ren Fail 44: 790-805, 2022.
9. Cadenas S: Mitochondrial uncoupling, ROS generation and cardioprotection. Biochim Biophys Acta Bioenerg 1859: 940-950, 2018.
10. Han Y, Xu X, Tang C, Gao P, Chen X, Xiong X, Yang M, Yang S, Zhu X, Yuan S, *et al*: Reactive oxygen species promote tubular injury in diabetic nephropathy: The role of the mitochondrial ros-txnip-nlrp3 biological axis. Redox Biol 16: 32-46, 2018.
11. Palomba H, Castro I, Yu L and Burdmann EA: The duration of acute kidney injury after cardiac surgery increases the risk of long-term chronic kidney disease. J Nephrol 30: 567-572, 2017.
12. Wei J, Zhang J, Wang L, Jiang S, Fu L, Buggs J and Liu R: New mouse model of chronic kidney disease transitioned from ischemic acute kidney injury. Am J Physiol Renal Physiol 317: F286-F295, 2019.
13. Zhang X, Agborbesong E and Li X: The role of mitochondria in acute kidney injury and chronic kidney disease and its therapeutic potential. Int J Mol Sci 22: 11253, 2021.
14. Jiang M, Bai M, Lei J, Xie Y, Xu S, Jia Z and Zhang A: Mitochondrial dysfunction and the AKI-to-CKD transition. Am J Physiol Renal Physiol 319: F1105-F1116, 2020.

15. Kang W, Suzuki M, Saito T and Miyado K: Emerging role of TCA cycle-related enzymes in human diseases. Int J Mol Sci 22: 13057, 2021.
16. Jourdain AA, Begg BE, Mick E, Shah H, Calvo SE, Skinner OS, Sharma R, Blue SM, Yeo GW, Burge CB and Mootha VK: Loss of LUC7L2 and U1 snRNP subunits shifts energy metabolism from glycolysis to OXPHOS. Mol Cell 81: 1905-1919.e12, 2021.
17. Fuller GG and Kim JK: Compartmentalization and metabolic regulation of glycolysis. J Cell Sci 134: jcs258469, 2021.
18. Livak KJ and Schmittgen TD: Analysis of relative gene expression data using real-time quantitative PCR and the 2(-Delta Delta C(T)) method. Methods 25: 402-408, 2001.
19. Love MI, Huber W and Anders S: Moderated estimation of fold change and dispersion for RNA-seq data with DESeq2. Genome Biol 15: 550, 2014.
20. Huss JM and Kelly DP: Nuclear receptor signaling and cardiac energetics. Circ Res 95: 568-578, 2004.
21. Zhang Q, Luo P, Chen J, Yang C, Xia F, Zhang J, Tang H, Liu D, Gu L, Shi Q, *et al*: Dissection of targeting molecular mechanisms of aristolochic acid-induced nephrotoxicity via a combined deconvolution strategy of chemoproteomics and metabolomics. Int J Biol Sci 18: 2003-2017, 2022.
22. Kanehisa M: Toward understanding the origin and evolution of cellular organisms. Protein Sci 28: 1947-1951, 2019.
23. Kanehisa M, Furumichi M, Sato Y, Kawashima M and Ishiguro-Watanabe M: KEGG for taxonomy-based analysis of pathways and genomes. Nucleic Acids Res 51: D587-D592, 2023.
24. Nissanka N and Moraes CT: Mitochondrial DNA damage and reactive oxygen species in neurodegenerative disease. FEBS Lett 592: 728-742, 2018.
25. Kan C, Ungelenk L, Lupp A, Dirsch O and Dahmen U: Ischemia-reperfusion injury in aged livers-the energy metabolism, inflammatory response, and autophagy. Transplantation 102: 368-377, 2018.
26. Vallée A, Guillevin R and Vallée JN: Vasculogenesis and angiogenesis initiation under normoxic conditions through Wnt/β-catenin pathway in gliomas. Rev Neurosci 29: 71-91, 2018.
27. May JL, Kouri FM, Hurley LA, Liu J, Tommasini-Ghelfi S, Ji Y, Gao P, Calvert AE, Lee A, Chandel NS, *et al*: IDH3α regulates one-carbon metabolism in glioblastoma. Sci Adv 5: eaat0456, 2019.
28. Findlay AS, Carter RN, Starbuck B, McKie L, Nováková K, Budd PS, Keighren MA, Marsh JA, Cross SH, Simon MM, *et al*: Mouse Idh3a mutations cause retinal degeneration and reduced mitochondrial function. Dis Model Mech 11: dmm036426, 2018.
29. Lambeth DO, Tews KN, Adkins S, Frohlich D and Milavetz BI: Expression of two succinyl-CoA synthetases with different nucleotide specificities in mammalian tissues. J Biol Chem 279: 36621-36624, 2004.
30. Donti TR, Stromberger C, Ge M, Eldin KW, Craigen WJ and Graham BH: Screen for abnormal mitochondrial phenotypes in mouse embryonic stem cells identifies a model for succinyl-CoA ligase deficiency and mtDNA depletion. Dis Model Mech 7: 271-280, 2014.
31. Kohno S, Linn P, Nagatani N, Watanabe Y, Kumar S, Soga T and Takahashi C: Pharmacologically targetable vulnerability in prostate cancer carrying RB1-SUCLA2 deletion. Oncogene 39: 5690-5707, 2020.
32. Shimozawa Y, Himiyama T, Nakamura T and Nishiya Y: Structural analysis and reaction mechanism of malate dehydrogenase from Geobacillus stearothermophilus. J Biochem 170: 97-105, 2021.
33. Gray LR, Tompkins SC and Taylor EB: Regulation of pyruvate metabolism and human disease. Cell Mol Life Sci 71: 2577-2604, 2014.
34. Laemmle A, Steck AL, Schaller A, Kurth S, Perret Hoigné E, Felser AD, Slavova N, Salvisberg C, Atencio M, Mochel F, *et al*: Triheptanoin-novel therapeutic approach for the ultra-rare disease mitochondrial malate dehydrogenase deficiency. Mol Genet Metab Rep 29: 100814, 2021.
35. Bergman O and Ben-Shachar D: Mitochondrial oxidative phosphorylation system (OXPHOS) deficits in schizophrenia: Possible interactions with cellular processes. Can J Psychiatry 61: 457-469, 2016.
36. Haapanen O, Reidelbach M and Sharma V: Coupling of quinone dynamics to proton pumping in respiratory complex I. Biochim Biophys Acta Bioenerg 1861: 148287, 2020.
37. Grivennikova VG, Gladyshev GV and Vinogradov AD: Deactivation of mitochondrial NADH:ubiquinone oxidoreductase (respiratory complex I): Extrinsically affecting factors. Biochim Biophys Acta Bioenerg 1861: 148207, 2020.
38. Zhu J, Vinothkumar KR and Hirst J: Structure of mammalian respiratory complex I. Nature 536: 354-358, 2016.
39. Rak M and Rustin P: Supernumerary subunits NDUFA3, NDUFA5 and NDUFA12 are required for the formation of the extramembrane arm of human mitochondrial complex I. FEBS Lett 588: 1832-1838, 2014.
40. Mimaki M, Wang X, McKenzie M, Thorburn DR and Ryan MT: Understanding mitochondrial complex I assembly in health and disease. Biochim Biophys Acta 1817: 851-862, 2012.
41. Chen Q, Thompson J, Hu Y, Dean J and Lesnefsky EJ: Inhibition of the ubiquitous calpains protects complex I activity and enables improved mitophagy in the heart following ischemia-reperfusion. Am J Physiol Cell Physiol 317: C910-C921, 2019.
42. Heidari E, Rasoulinezhad M, Pak N, Reza Ashrafi M, Heidari M, Banwell B, Garshasbi M and Reza Tavasoli A: Defective complex III mitochondrial respiratory chain due to a novel variant in CYC1 gene masquerades acute demyelinating syndrome or leber hereditary optic neuropathy. Mitochondrion 60: 12-20, 2021.
43. Sánchez E, Lobo T, Fox JL, Zeviani M, Winge DR and Fernández-Vizarra E: LYRM7/MZM1L is a UQCRFS1 chaperone involved in the last steps of mitochondrial complex III assembly in human cells. Biochim Biophys Acta 1827: 285-293, 2013.
44. Gusic M, Schottmann G, Feichtinger RG, Du C, Scholz C, Wagner M, Mayr JA, Lee CY, Yépez VA, Lorenz N, *et al*: Bi-allelic UQCRFS1 variants are associated with mitochondrial complex III deficiency, cardiomyopathy, and alopecia totalis. Am J Hum Genet 106: 102-111, 2020.
45. Wang Q, Li M, Gan Y, Jiang S, Qiao J, Zhang W, Fan Y, Shen Y, Song Y, Meng Z, *et al*: Mitochondrial protein UQCRC1 is oncogenic and a potential therapeutic target for pancreatic cancer. Theranostics 10: 2141-2157, 2020.
46. Zeng J, Tao J, Xi L, Wang Z and Liu L: PCSK9 mediates the oxidative low-density lipoprotein-induced pyroptosis of vascular endothelial cells via the UQCRC1/ROS pathway. Int J Mol Med 47: 53, 2021.
47. Giannos P, Prokopidis K, Raleigh SM, Kelaiditi E and Hill M: Altered mitochondrial microenvironment at the spotlight of musculoskeletal aging and Alzheimer's disease. Sci Rep 12: 11290, 2022.
48. Han Y, Sun S, Zhao M, Zhang Z, Gong S, Gao P, Liu J, Zhou J, Ma D, Gao Q and Wu P: CYC1 predicts poor prognosis in patients with breast cancer. Dis Markers 2016: 3528064, 2016.
49. Oka SI, Hsu CP and Sadoshima J: Regulation of cell survival and death by pyridine nucleotides. Circ Res 111: 611-627, 2012.
50. Yang Y and Sauve AA: NAD(+) metabolism: Bioenergetics, signaling and manipulation for therapy. Biochim Biophys Acta 1864: 1787-1800, 2016.
51. Ying W: NAD+/NADH and NADP+/NADPH in cellular functions and cell death: Regulation and biological consequences. Antioxid Redox Signal 10: 179-206, 2008.
52. Shi F, Zhang Z, Wang J, Wang Y, Deng J, Zeng Y, Zou P, Ling X, Han F, Liu J, *et al*: Analysis by metabolomics and transcriptomics for the energy metabolism disorder and the Aryl hydrocarbon receptor activation in male reproduction of mice and GC-2spd cells exposed to $PM_{2.5}$. Front Endocrinol (Lausanne) 12: 807374, 2022.
53. Chouchani ET, Pell VR, James AM, Work LM, Saeb-Parsy K, Frezza C, Krieg T and Murphy MP: A unifying mechanism for mitochondrial superoxide production during ischemia-reperfusion injury. Cell Metab 23: 254-263, 2016.
54. Baldissera MD, Souza CF, Grings M, Parmeggiani BS, Leipnitz G, Moreira KLS, da Rocha MIUM, da Veiga ML, Santos RCV, Stefani LM and Baldisserotto B: Inhibition of the mitochondrial respiratory chain in gills of Rhamdia quelen experimentally infected by Pseudomonas aeruginosa: Interplay with reactive oxygen species. Microb Pathog 107: 349-353, 2017.
55. Zhao M, Wang Y, Li L, Liu S, Wang C, Yuan Y, Yang G, Chen Y, Cheng J, Lu Y and Liu J: Mitochondrial ROS promote mitochondrial dysfunction and inflammation in ischemic acute kidney injury by disrupting TFAM-mediated mtDNA maintenance. Theranostics 11: 1845-1863, 2021.
56. Hessam S, Gambichler T, Skrygan M, Sand M, Rüddel I, Scholl L and Bechara FG: Reduced ten-eleven translocation and isocitrate dehydrogenase expression in inflammatory hidradenitis suppurativa lesions. Eur J Dermatol 28: 449-456, 2018.

57. Alkhater RA, Ahonen S and Minassian BA: SUCLA2 Arg407Trp mutation can cause a nonprogressive movement disorder-deafness syndrome. Ann Clin Transl Neurol 8: 252-258, 2021.
58. Pei X, Li KY, Shen Y, Li JT, Lei MZ, Fang CY, Lu HJ, Yang HJ, Wen W, Yin M, *et al*: Palmitoylation of MDH2 by ZDHHC18 activates mitochondrial respiration and accelerates ovarian cancer growth. Sci China Life Sci 65: 2017-2030, 2022.
59. Chen J, Jin J, Zhang X, Yu H, Zhu X, Yu L, Chen Y, Liu P, Dong X, Cao X, *et al*: Microglial lnc-U90926 facilitates neutrophil infiltration in ischemic stroke via MDH2/CXCL2 axis. Mol Ther 29: 2873-2885, 2021.
60. Ma Q, Wang C, Wang M, Li Y, Li P, Wang J, Cheng L, An Y, Dai H, Duan Y, *et al*: Investigation of brain damage mechanism in middle cerebral artery occlusion/reperfusion rats based on i-TRAQ quantitative proteomics. Exp Brain Res 239: 1247-1260, 2021.
61. Wang B, Li ZL, Zhang YL, Wen Y, Gao YM and Liu BC: Hypoxia and chronic kidney disease. EBioMedicine 77: 103942, 2022.